High-throughput platform of reconstituted depolarization-induced Ca^{2+} release for skeletal muscle disease mutation validation and drug discovery

Takashi Murayama[1*], Nagomi Kurebayashi[1], Takuro Numaga-Tomita[2], Takuya Kobayashi[1], Satoru Okazaki[1], Kyosuke Yamashiro[1], Tsutomu Nakada[2], Shuichi Mori[3], Ryosuke Ishida[3], Hiroyuki Kagechika[3], Mitsuhiko Yamada[2], Takashi Sakurai[1]

[1]Department of Pharmacology, Juntendo University School of Medicine, Tokyo, Japan.

[2]Department of Molecular Pharmacology, Shinshu University School of Medicine, Matsumoto, Japan.

[3]Institute of Biomaterials and Bioengineering, Tokyo Medical and Dental University, Tokyo, Japan.

Short running title: High-throughput platform for reconstituted DICR

[*]Corresponding author: Takashi Murayama, Ph.D., Department of Pharmacology, Juntendo University School of Medicine, Tokyo 113-8421, Japan. E-mail: takashim@juntendo.ac.jp

Summary

Mutations in essential components for depolarization-induced Ca^{2+} release (DICR) are implicated into various skeletal muscle diseases. Murayama et al. establish high-throughput platform for the reconstituted DICR in nonmuscle cells for evaluation of disease-causing mutations and drug discovery.

Abstract

In skeletal muscle excitation-contraction (E-C) coupling, depolarization of the plasma membrane triggers Ca^{2+} release from the sarcoplasmic reticulum (SR), referred to as depolarization-induced Ca^{2+} release (DICR). DICR occurs via the type 1 ryanodine receptor (RyR1), which physically interacts with the dihydropyridine receptor Cav1.1 subunit in specific machinery formed with additional essential components including β1a, Stac3 adaptor protein and junctophilins. Exome sequencing has accelerated the discovery of many novel mutations in DICR machinery genes in various skeletal muscle diseases. However, functional validation is time-consuming because it must be performed in a skeletal muscle environment. In this study, we established a high-throughput platform of the reconstituted DICR in HEK293 cells. The essential components were effectively transduced into HEK293 cells expressing RyR1 using baculovirus vectors, and Ca^{2+} release was quantitatively measured with R-CEPIA1er, a fluorescent ER Ca^{2+} indicator, without contaminant of extracellular Ca^{2+} influx. In these cells, $[K^+]$-dependent Ca^{2+} release was triggered by chemical depolarization with the aid of inward rectifying potassium channel, indicating a successful reconstitution of DICR. Using the platform, we evaluated several Cav1.1 mutations that are implicated in malignant hyperthermia and myopathy. We also tested several RyR1 inhibitors; whereas dantrolene and Cpd1 inhibited DICR, procaine had no effect. Furthermore, twitch potentiators such as perchlorate and thiocyanate accelerated DICR without affecting Ca^{2+}-induced Ca^{2+} release. These results well reproduced the findings with the muscle fibers and the cultured myotubes. This high-throughput DICR platform will be highly useful for validation of mutations and drug discovery for skeletal muscle diseases.

Introduction

In vertebrate skeletal muscle, depolarization of the plasma membrane triggers Ca^{2+} release from the sarcoplasmic reticulum (SR), which is commonly referred to as excitation-contraction (E-C) coupling. This process occurs at triad junctions in which a transverse (T) tubule is closely apposed to terminal cisterna of the SR(Franzini-Armstrong, 2018). In excitation-contraction coupling, the type 1 ryanodine receptor (RyR1), a Ca^{2+} release channel in the SR, is activated by a conformational change of the voltage sensor in the Cav1.1 subunit of the dihydropyridine receptor (DHPR) upon depolarization of the T-tubule membrane. This is referred to as depolarization-induced Ca^{2+} release (DICR)(Rios and Pizarro, 1991; Schneider, 1994). Studies with knockout animals have revealed that functional and structural interactions between Cav1.1 and RyR1 in muscle require at least three additional components, a β1a auxiliary subunit of DHPR(Flucher and Campiglio, 2019; Shishmarev, 2020), the Stac3 adaptor protein(Horstick et al., 2013; Nelson et al., 2013; Reinholt et al., 2013), and junctophilins(Takeshima et al., 2000), which may form specific machinery for DICR(Flucher and Campiglio, 2019; Shishmarev, 2020; Rufenach and Van Petegem, 2021).

Mutations in genes that encode DICR machinery components have been implicated in various types of muscle diseases, including congenital myopathies, periodic paralysis, and malignant hyperthermia (MH)(Agrawal et al., 2018; Flucher, 2020; Lawal et al., 2020). Rapid exome sequencing has accelerated the discovery of novel mutations; however, validation of these mutations by functional testing is critically important for the diagnosis and treatment of these diseases. This has been performed using myotubes from mice that lack DICR machinery components, for example knockout mice of Cav1.1(Tanabe et al., 1988), β1a(Gregg et al., 1996) and Stac3(Polster et al., 2016). While this approach has evaluated several disease-causing mutations in the DICR components (Weiss et al., 2004; Pirone et al., 2010; Eltit et al., 2012; Polster et al., 2016; Perez et al., 2018), it has certain limitations. For example, it is expensive and labor intensive to maintain the mouse lines. Differentiation of cells into myotubes is time consuming and is affected by various factors, such as the cell line used and experimental conditions. Furthermore, transduction of foreign genes into myotubes is often inefficient.

There are no specific treatments for most diseases related to mutations in the DICR machinery. A major cause for the slow pace of novel drug development is the lack of an appropriate drug screening platform for these diseases. We have recently established an efficient high-throughput platform for screening RyR1-targeted drugs using endoplasmic reticulum (ER)

Ca^{2+} measurements in HEK293 cells(Murayama et al., 2018; Murayama and Kurebayashi, 2019) and using this platform we developed Compound 1 (Cpd1), a novel RyR1 inhibitor for treatment of MH(Mori et al., 2019; Yamazawa et al., 2021). Therefore, functional screening using HEK293 cells is a promising platform for drug discovery.

Recently, Perni et al. successfully reconstituted DICR by co-expressing five essential components, RyR1, Cav1.1, β1a, junctophilin-2 (JP2) and Stac3, in non-muscle tsA201 cells(Perni et al., 2017). They demonstrated formation of ER-plasma membrane junctions in which Cav1.1 is arranged into tetrads, which is indicative of physical links to RyR1(Block et al., 1988). Depolarization of the plasma membrane using the patch-clamp technique induced a rapid Ca^{2+} transient without influx of extracellular Ca^{2+}. This provides a basis for developing reconstituted DICR.

In this study, we established a high-throughput platform for DICR that was reconstituted in HEK293 cells. Baculovirus infection of essential components greatly improved transduction efficiency. Chemical depolarization by high concentration potassium [K^+] solutions with the aid of an inward-rectified potassium channel (Kir2.1) enabled the simultaneous stimulation of many cells. Furthermore, a genetically-encoded ER Ca^{2+} indicator quantitatively measured DICR without influence of extracellular Ca^{2+} influx. Using this platform, we successfully evaluated disease-causing mutations in Cav1.1 and tested several RyR1 inhibitors and DICR modulators. Our high-throughput platform will accelerate the validation of mutations and drug discovery for skeletal muscle diseases.

Materials and Methods

Generation of stable inducible HEK293 cell lines

HEK293 cells stably expressing R-CEPIA1er and RyR1 were generated as described previously(Murayama et al., 2018; Murayama and Kurebayashi, 2019). Briefly, a full-length rabbit RyR1 cDNA was cloned in a tetracycline-induced expression vector (pcDNA5/FRT/TO; Life Technologies, CA, USA)(Tong et al., 1997). Flp-In T-REx HEK293 cells were co-transfected with this expression vector and pOG44 in accordance with the manufacturer's instructions. Clones with suitable doxycycline-induced expression of RyR1 were selected and used for experiments. The cells were then transfected with an R-CEPIA1er cDNA (a generous gift from Masamitsu Iino, The University of Tokyo) for stable expression of R-CEPIA1er. Cells were cultured in Dulbecco's modified Eagle's medium supplemented with 10% fetal calf serum,

112 2 mM L-glutamine, 15 μg/ml blasticidin, and 100 μg/ml hygromycin.

113 **Production of baculovirus**

114 Baculovirus that expresses vesicular stomatitis virus G-protein (VSVG) on the virus
115 envelope(Tani et al., 2001) was produced using the Bac-to-Bac system (LifeTechnologies) as
116 described previously(Uehara et al., 2017). cDNAs for Cav1.1, β1a, JP2, Stac3, and Kir2.1 were
117 cloned from mouse skeletal muscle using reverse transcription-PCR (primers pair are listed in
118 **Table 1**) and cloned into the modified donor vector (pFastBac1-VSVG-CMV-WPRE).
119 Baculovirus was produced in Sf9 cells according to the manufacturer's instructions
120 (LifeTechnologies). Baculovirus titers were immunologically determined using an anti-gp64
121 antibody (AcV5, Santa Cruz Biotechnology)(Kitts and Green, 1999). Titers were 1–2×10^8
122 pfu/mL for all viruses. The baculovirus solutions were stored in the dark at 4°C and used within
123 one month after production.

124 **Immunocytochemistry**

125 RyR1-HEK293 cells infected with baculovirus for the essential components (5 BV cells) were
126 fixed with ice-cold methanol and rinsed with phosphate-buffered saline (PBS). The cells were
127 blocked with 5% BSA/PBS for 30 min and incubated overnight with primary antibodies against
128 Cav1.1 (sc-514685, Santa Cruz Biotechnology), β1a (MA5-27714, Invitrogen), JP2 (sc-377086,
129 Santa Cruz Biotechnology), Stac3 (1G8, Abnova), or Kir2.1 (S112B-14, Invitrogen) in 1%
130 BSA/PBS. After washing three times with PBS, the cells were incubated for 2 h with Alexa594-
131 labeled goat anti-mouse IgG (Invitrogen) in 1% BSA/PBS. After washing with PBS, the cells
132 were observed using an all-in-one fluorescence microscope (BZ-X710, Keyence, Osaka, Japan).

133 **Western blotting**

134 RyR1-HEK293 cells with or without baculovirus infection for the essential components were
135 lysed with Pro-Prep protein extraction solution (iNtRON Biotechnology). The extracted
136 proteins were separated on 3–15% polyacrylamide gels and transferred to PVDF membranes.
137 Membranes were probed with the primary antibodies described above, followed by HRP-
138 labeled anti-mouse IgG (04-18-18, KPL). Positive bands were detected by chemiluminescence
139 using ImmunoStar LD (Fujifilm Wako Chemicals) as a substrate.

140 **Single-cell Ca^{2+} imaging**

141 RyR1/R-CEPPIA1er HEK293 cells grown on a glass-bottomed dish were treated with
142 doxycycline to induce the expression of RyR1 and infected with 5 BV 24 h prior to
143 measurement. Single-cell Ca^{2+} imaging was performed as described previously(Murayama et
144 al., 2015; Uehara et al., 2017). Measurements were performed at 26°C by perfusing solutions
145 using an in-line solution heater/cooler (Warner Instruments, Holliston, MA, USA). ER [Ca^{2+}]
146 signals were determined by R-CEPIA1er fluorescence excited at 561 nm using a 40× objective
147 lens. Cells were perfused with normal Krebs solution (140 mM NaCl, 5 mM KCl, 2 mM $CaCl_2$,
148 1 mM $MgCl_2$, 11 mM glucose, 5 mM HEPES, pH 7.4) for 30 s, high [K^+] Krebs solution
149 containing 50 mM [K^+] for 50 s, and normal Krebs solution for 1.5 min. Fluorescence intensities
150 in individual cells were determined by region of interest (ROI) analysis using AquaCosmos
151 software (Hamamatsu Photonics, Hamamatsu, Japan).

152 **Time lapse ER [Ca^{2+}] Measurements using a fluorometer**

153 Time lapse ER [Ca^{2+}] measurements were performed using the FlexStation3 fluorometer
154 (Molecular Devices, San Jose, CA)(Murayama et al., 2018; Murayama and Kurebayashi, 2019).
155 Stable RyR1/R-CEPIA1er HEK293 cells were seeded on 96-well flat-, clear-bottom black
156 microplates (#3603, Corning, New York, NY) at a density of 3×10^4 cells/well in 100 μL culture
157 medium. One day after seeding, 100 μL culture medium containing 2 μg/mL doxycycline (for
158 induction of RyR1) and baculovirus solutions for Cav1.1, β1a, JP2, Stac3, and Kir2.1 (2 μL
159 each) were added to each well. After 24 h, the culture medium were replaced with 81 μL normal
160 Krebs solution, and the microplate was placed in a FlexStation3 fluorometer preincubated at
161 37°C. Signals from R-CEPIA1er, which was excited at 560 nm and emitted at 610 nm, were
162 captured every 5 seconds for 150 seconds. Thirty seconds after starting, 54 μL of the high [K^+]
163 or caffeine solution was applied to the cells. The fluorescence change was expressed as F/F_0 in
164 which averaged fluorescence intensity of the last 25 seconds (F) was normalized to that of the
165 initial 25 seconds (F_0). For drug testing, compounds were added to normal Krebs solution at
166 the indicated concentrations.

167 For determination of resting ER [Ca^{2+}], cells were incubated with 81 μL normal Krebs
168 solution, and 54 μL Krebs solution containing 50 mM Ca^{2+} and 50 μM ionomycin was added
169 30 sec after starting (final concentrations of Ca^{2+} and ionomycin were 20 mM and 20 μM,
170 respectively). R-CEPIA1er fluorescence was captured every 10 seconds for 6 min.

171 **Measurement of resting membrane potential**

172 The resting membrane potential of baculovirus-infected RyR1-HEK293 cells with or without

173 Kir2.1 expression was measured under current-clamp conditions in the whole cell configuration
174 of the patch-clamp method with an Axopatch 200B amplifier (Molecular Devices, San Jose,
175 CA). Pipettes were fabricated from borosilicate glass capillaries (Kimble) with a vertical pipette
176 puller (PP-83, Narishige, Tokyo, Japan). Pipettes had series resistance of 3–4 MΩ when filled
177 with the pipette solution containing (in mM) 120 D-glutamate, 20 KCl, 10 NaCl, 0.1 EGTA, 2
178 $MgCl_2$, 3 MgATP, and 5 Hepes (pH 7.4 adjusted with KOH). The series resistance was routinely
179 compensated by ~75% with the amplifier. Bath solution contained (in mM): 140 NaCl, 5 KCl,
180 11 glucose, 2 $CaCl_2$, 1 $MgCl_2$, and 10 Hepes (pH 7.4 adjusted with NaOH). High [K^+] bath
181 solution contained (in mM): 95 NaCl, 50 KCl, 11 glucose, 2 $CaCl_2$, 1 $MgCl_2$, and 10 Hepes (pH
182 7.4 adjusted with NaOH). The resting membrane potential was measured immediately after
183 breaking into cells.

184 **Statistics**

185 Data are presented as means ± SD. Unpaired Student's t test was used for comparisons between
186 two groups. One-way analysis of variance (ANOVA), followed by Dunnett's test, was
187 performed to compare three or more groups. Two-tailed tests were used for all analyses.
188 Statistical analysis was performed using Prism v9 (GraphPad Software, Inc., La Jolla, USA).

189 **Results**

190 **Establishment of a high-throughput platform for DICR using a fluorescence microplate**
191 **reader**

192 To reconstitute DICR, we used HEK293 cells stably expressing RyR1 and R-
193 CEPIA1er, a genetically-encoded fluorescent ER Ca^{2+} indicator(Suzuki et al., 2014), that were
194 generated for high-throughput screening of novel RyR1 inhibitors(Murayama et al., 2018;
195 Murayama and Kurebayashi, 2019) (**Fig. 1 A**, left). The other components for DICR, Cav1.1,
196 β1a, Stac3 and JP2, which were used by Perni et al.(Perni et al., 2017), were transduced using
197 VSV-G pseudotyped baculovirus (BV), which efficiently infects mammalian cells(Tani et al.,
198 2001; Uehara et al., 2017) (**Fig. 1 A**, right). In these cells, DICR can be detected by a decrease
199 in ER Ca^{2+}. To prevent extracellular Ca^{2+} influx through Cav1.1 by depolarization, a N617D
200 mutation was introduced that abolishes Ca^{2+} conductance(Schredelseker et al., 2010). In
201 addition, we expressed Kir2.1, an inward-rectified potassium channel in skeletal
202 muscle(DiFranco et al., 2015), to hyperpolarize the membrane potential because the resting
203 membrane potential in HEK293 cells is much less (−20 mV) than in skeletal muscle (−90

204 mV)(Kirkton and Bursac, 2011). Imunocytochemistry revealed that the five proteins (Cav1.1,
205 β1a, Stac3, JP2, and Kir2.1) were successfully expressed in almost all cells, which we term
206 hereafter 5 BV cells (**Fig. S1 A**). BV-dependent protein expression was also confirmed by
207 western blotting of cell lysate (**Fig. S1 B**). Therefore, BV infection effectively transduced the
208 essential components of DICR in RyR1/R-CEPIA1er-HEK293 cells.

209 To detect DICR, we used a fluorescence microplate reader (FlexStation3), which
210 measures time-lapse R-CEPIA1er fluorescence in 96-well plates. Fluorescence signals were
211 collected in a 1.5 mm diameter area; therefore, an averaged signal from thousands of cells was
212 detected in each well. We adopted chemical depolarization using high [K^+] solutions, which
213 can simultaneously depolarize all the cells to trigger DICR. The cells were initially incubated
214 with normal Krebs solution containing 5 mM [K^+]. Then, solutions containing various [K^+]
215 concentrations were added to give [K^+] concentrations of 5–61 mM. In cells without BV
216 infection, no apparent changes in fluorescence were observed with any [K^+] concentration (**Fig.
217 1 B**, left). Caffeine (10 mM) reduced the R-CEPIA1er fluorescence, confirming the functional
218 expression of RyR1. In 5 BV cells, high [K^+] solution rapidly reduced the R-CEPIA1er
219 fluorescence in a [K^+]-dependent manner (**Fig. 1 B**, right). To monitor ER Ca^{2+} changes in
220 individual cells, we also observed R-CEPIA1er fluorescence using laser scanning confocal
221 microscopy. In 5 BV cells, high [K^+] solution caused a large and transient reduction in the R-
222 CEPIA1er fluorescence in 90% of cells (**Movie S1** and **Fig. S2**).

223 For quantitative analysis, we normalized the averaged fluorescence intensity of the last
224 25 seconds (F) to that of the initial 25 seconds (F_0) to correct variations in the initial
225 fluorescence intensity between wells. The F/F_0 plot as a function of [K^+] concentrations
226 demonstrated [K^+] dependence with an EC_{50} of 9.8 ± 0.1 mM [K^+] (**Fig. 1 C**). The initial
227 fluorescence change after stimulation (i.e., 35 seconds), which may reflect the rate of Ca^{2+}
228 release, provided larger EC_{50} (17.0 ± 0.4 mM). However, variations were larger, especially near
229 EC_{50} value because of rapid changes in fluorescence intensity (**Fig. 1 C**). The fluorescence
230 change by 61 mM [K^+], which is expressed as $1-F/F_0$ (**Fig. 1 C**), reached ~80% of that induced
231 by caffeine in 5 BV cells, indicating a high degree of DICR reconstitution (**Fig. 1 D**). Taken
232 together, these results indicate successful establishment of a high-throughput platform for DICR.

233 The original method for DICR reconstitution monitors cytoplasmic [Ca^{2+}](Perni et al.,
234 2017); therefore, we also assessed DICR by measuring cytoplasmic Ca^{2+} using G-GECO1.1, a
235 genetically-encoded Ca^{2+} indicator(Zhao et al., 2011). In cells without BV infection, a

236 substantial increase in [Ca^{2+}] was observed by high [K^+], indicating the existence of endogenous
237 Ca^{2+} influx pathways by depolarization (**Fig. S3 A**). In 5 BV cells, DICR was detected by rapid
238 and large increases in [Ca^{2+}], which declined with time (**Fig. S3 B**). The initial fluorescence
239 change after stimuli (i.e., 35 seconds) provided dose-dependent curve with EC_{50} of 16.4 ± 0.5
240 mM, which is similar to the value determined by initial fluorescence change in ER Ca^{2+}
241 measurement (see **Fig. 1 C**).

242 **Validation of the reconstituted DICR**

243 We next determined whether the reconstituted platform reproduces DICR in skeletal
244 muscle. Initially, we examined the role of the essential components. Removal of Cav1.1 resulted
245 in complete loss of high [K^+]-induced Ca^{2+} release (**Fig. 2A-C**). Ca^{2+} release was also lost in
246 cells lacking β1a or Stac3, and in cells expressing RyR2 instead of RyR1 (**Fig. 2 C**). Removal
247 of JP2 significantly reduced the fluorescence change by 61 mM [K^+] with a large rightward
248 shift in [K^+] dependence (**Fig. 2 B, C**). These results are consistent with previous findings of
249 mice lacking each component(Tanabe et al., 1988; Takeshima et al., 1994; Gregg et al., 1996;
250 Takeshima et al., 2000; Polster et al., 2016).

251 Skeletal muscle Cav1.1 forms a complex with three auxiliary subunits, β1a, α_2-δ and
252 γ_1(Catterall, 2000). α_2-δ and γ_1 may play modulatory roles(Flucher et al., 2005). Additional
253 expression of α_2-δ had no effect on high [K^+]-induced Ca^{2+} release (**Fig. 2 D, E**). Expression of
254 γ1 did not significantly affect high [K^+]-induced Ca^{2+} release at 20 mM or lower [K^+] but it
255 reduced the fluorescence change at higher [K^+] concentrations (**Fig. 2 D, E**). In γ_1 cells, R-
256 CEPIA1er fluorescence decreased but increased again with time, suggesting inactivation of the
257 Ca^{2+} release (**Fig. 2 A**). These findings are consistent with previous reports of the effects of α_2-
258 δ(Obermair et al., 2005) and γ_1(Ursu et al., 2004) on DICR. Therefore, our reconstituted
259 platform can reproduce DICR in skeletal muscle and is valid for evaluating disease-causing
260 mutations or drugs.

261 We also tested the importance of Kir2.1 on the reconstituted DICR platform. We
262 measured membrane potential of cells under current-clamp conditions using pipette solution
263 containing ~145 mM [K^+] (**Fig. 3 A**). The membrane potential of 5 BV-infected cells was -71
264 ± 3 mV in normal Krebs solution and became depolarized to -14 ± 3 mV by high [K^+] solution
265 containing 50 mM [K^+]. In contrast, membrane potential was already depolarized in the cells
266 without Kir2.1 (-18 ± 2 mV) in normal Krebs solution, which is consistent with the previous
267 report(Kirkton and Bursac, 2011). Without Kir2.1, R-CEPIA1er fluorescence intensity was

268 substantially reduced and high [K^+]-induced Ca^{2+} release was completely abolished (**Fig. 3 B**).
269 We quantified resting ER [Ca^{2+}] by determining the maximum fluorescence intensity of R-
270 CEPIA1er using ionomycin/Ca^{2+} (**Fig. 3 C**). The resting ER [Ca^{2+}] was severely reduced in
271 cells without Kir2.1 (**Fig. 3 D**). These results suggest that persistently activated DICR activity
272 under the depolarized conditions causes ER Ca^{2+} depletion. In support of this, further removal
273 of β1a or Stac3, which completely abolishes DICR activity, restored the ER [Ca^{2+}] (**Fig. 3 D**).
274 Therefore, Kir2.1 is indispensable for our reconstituted DICR platform.

275 **Evaluation of disease-causing mutations in Cav1.1**

276 Using the high-throughput DICR platform, we evaluated mutations in Cav1.1 which
277 are implicated in various muscle diseases(Beam et al., 2017; Flucher, 2020). We initially tested
278 known MH mutations, R174W(Carpenter et al., 2009), R1086H(Stewart et al., 2001), and
279 T1354S(Pirone et al., 2010) (**Fig. 4 A**). We found that ER [Ca^{2+}] was severely reduced for
280 R1086H (**Fig. 4 B**) and that R1086H exhibited a smaller fluorescence change in response to
281 high [K^+] (**Fig. 4 C, D**) compared with the wild type (WT) or the other mutants. This was partly
282 caused by low ER [Ca^{2+}], which reduces maximum fluorescence changes. In addition, R1086H
283 showed an enhanced [K^+]-dependence, i.e., lower EC_{50} value for [K^+] (**Fig. 4 C, E**). In contrast,
284 no or only minor changes in ER [Ca^{2+}] and [K^+] dependence were observed for R174W and
285 T1354S cells (**Fig. 4 B–E**). We anticipated that the reduction in ER [Ca^{2+}] in R1086H cells was
286 caused by activation of Cav1.1 at resting membrane potential because of its hypersensitivity.
287 To test the hypothesis, we hyperpolarized the membrane potential which reduced the activation
288 of Cav1.1. Reduction of [K^+] in the Krebs solution from 5 mM to 2.5 mM successfully
289 hyperpolarized the membrane potential by ~15 mV (**Fig. S4 A**). This substantially increased
290 ER [Ca^{2+}] in R1086H cells to a level comparable to that in WT cells (**Fig. S4 B**). R1086H cells
291 exhibited a clear greater sensitivity to [K^+] than WT cells (**Fig. S4 C–E**), supporting our
292 hypothesis of R1086H hyperactivation.

293 Previous functional characterization of these Cav1.1 mutants consistently showed
294 enhanced caffeine sensitivity, i.e., acceleration of Ca^{2+}-induced Ca^{2+} release (CICR)(Weiss et
295 al., 2004; Pirone et al., 2010; Eltit et al., 2012). We tested caffeine dependence of these mutants
296 in our platform. Caffeine released Ca^{2+} from WT cells in a dose-dependent manner (**Fig. 4 F**).
297 R1086H cells also exhibited a caffeine dependence but with reduced fluorescence change by
298 61 mM [K^+] (**Fig. 4 G**) and a significantly smaller EC_{50} (**Fig. 4 H**), indicating an enhanced
299 caffeine sensitivity. In contrast, caffeine dependence was not changed in R174W or T1354S

300 cells (**Fig. 4 F–H**).

301 We next examined the effect of myopathy-related mutations in Cav1.1 on DICR
302 activity. We chose four mutations, E100K, F275L, P742Q, and L1367V(Schartner et al., 2017),
303 none of which have been functionally characterized (**Fig. 5 A**). ER [Ca^{2+}] was not changed by
304 any of these mutations (**Fig. 5 B**). DICR activity was completely lost in the F275L mutant (**Fig.**
305 **5 C, D**) and there was a substantial rightward shift in [K^+] dependence for P742Q (**Fig. 5 C**);
306 The EC_{50} value was threefold higher in P742Q (33.2 ± 1.0 mM) compared with WT (10.3 ± 0.9
307 mM) (**Fig. 5 E**). The other two mutations (E100K and L1367V) had no significant effects on
308 [K^+] dependence (**Fig. 5 C-E**). We also tested the effects of these mutations on caffeine-induced
309 Ca^{2+} release. No substantial changes were observed with any of the mutations (**Fig. 5 F–H**).

310 **Effect of drugs on DICR activity**

311 The high-throughput DICR platform is expected to be useful for screening drugs for
312 muscle diseases. To test this possibility, we examined the effects of known DICR modulators.
313 We initially tested three RyR1 inhibitors (**Fig. 6 A**). Dantrolene is a well-known RyR1 inhibitor
314 that is clinically used for MH(Riazi et al., 2018). Cpd1 is a novel potent RyR1-selective
315 inhibitor that we recently developed(Mori et al., 2019; Yamazawa et al., 2021). Procaine
316 inhibits CICR but not DICR in frog skeletal muscle(Thorens and Endo, 1975; Kashiyama et al.,
317 2010). Dantrolene (10 μM) and Cpd1 (3 μM) caused rightward shifts in [K^+] dependence
318 compared with the control, indicating that they inhibit DICR (**Fig. 6 B, C**). This is consistent
319 with the suppression of twitch and tetanic tension in isolated muscles and with reduced *in vivo*
320 muscle weakness by dantrolene(Meyler et al., 1979; Leslie and Part, 1981) and
321 Cpd1(Yamazawa et al., 2021). Procaine (5 mM), in contrast, did not inhibit DICR (**Fig. 6 B,**
322 **C**). All three compounds shifted the caffeine dependence rightward, indicating inhibition of
323 CICR (**Fig. 6 D, E**). These results indicate that dantrolene and Cpd1 inhibit both DICR and
324 CICR, whereas procaine is a CICR-selective inhibitor.

325 Lyotropic anions, such as perchlorate and thiocyanate, potentiate E-C coupling in
326 skeletal muscle(Luttgau et al., 1983; Huang, 1986; Csernoch et al., 1987; Delay et al., 1990;
327 Gonzalez and Rios, 1993). Perchlorate (10 mM) and thiocyanate (10 mM) significantly shifted
328 the [K^+] dependence leftward (**Fig. 7 A, B**). In contrast, they did not affect caffeine dependence
329 (**Fig. 7 C, D**). These results indicate that lyotropic anions potentiate DICR but not CICR. This
330 is consistent with previous findings showing that the potentiating effects of lyotropic anions are
331 primarily caused by shifting voltage dependence of the charge movement toward more negative

332 potentials(Luttgau et al., 1983; Huang, 1986; Csernoch et al., 1987; Delay et al., 1990; Gonzalez
333 and Rios, 1993). Taken together, our high-throughput platform reproduces the effects of known
334 DICR modulators, indicating that it can be used to screen for and test drugs that affect DICR.

335 **Discussion**

336 In this study, we established a high-through platform for DICR that was reconstituted in
337 HEK293 cells expressing RyR1 and R-CEPIA1er. We made three key improvements to the
338 original method by Perni et al. (Perni et al., 2017). First, the essential components were
339 transduced using VSV-G pseudotyped baculovirus, which can effectively infect a wide variety
340 of mammalian cells without toxicity(Tani et al., 2001). This greatly increased the transduction
341 efficiency; almost all cells expressed the essential components (**Fig. S1**). Second,
342 depolarization of the plasma membrane was induced by high [K^+] solution. This enabled us to
343 simultaneously stimulate many cells (**Fig. 1, Fig. S2** and **movie S1**). For this purpose, we
344 expressed Kir2.1, an inward-rectifying potassium channel, which effectively hyperpolarized
345 the membrane potential (Kirkton and Bursac, 2011) (**Fig. 3**). Third, ER [Ca^{2+}], instead of
346 cytoplasmic [Ca^{2+}], was measured to detect DICR. This is critically important to avoid
347 contamination of signals from extracellular Ca^{2+} influx. Indeed, ER [Ca^{2+}] was not changed by
348 high [K^+] depolarization in cells without essential components (**Fig. 1 A**), in contrast to
349 substantial increases in cytoplasmic [Ca^{2+}] (**Fig. S4 A**). These improvements allow quantitative
350 measurements of DICR using a microplate reader.

351 In our reconstitution, five components, RyR1, Cav1.1, β1a, JP2 and Stac3, are essential for
352 DICR; removal of each component abolished or reduced the DICR activity (**Fig. 2 A, B**). This
353 is consistent with previous findings from mice lacking each component(Tanabe et al., 1988;
354 Takeshima et al., 1994; Gregg et al., 1996; Takeshima et al., 2000; Polster et al., 2016). In
355 addition, the effects of α_2-δ and γ_1 auxiliary subunits on DICR activity corresponded with
356 findings of previous reports (Ursu et al., 2004; Obermair et al., 2005) (**Fig. 2 C, D**). Therefore,
357 our reconstituted platform successfully reproduces DICR in skeletal muscle. We found that a
358 substantial DICR still occurred without JP2 (**Fig. 2 A, B**). This is in contrast to reports by Perni
359 et al.(Perni et al., 2017; Perni and Beam, 2022), in which no voltage-gated Ca^{2+} release was
360 observed in reconstituted cells without junctophilins. A possible reason for this is differences
361 in expression methods. Our VSV-G baculovirus is more effective at transduction than standard
362 lipofection; therefore, sufficient proteins were expressed that might spontaneously interact with
363 each other without junctophilins.

364 We quantitatively evaluated the effect of disease-casing mutations or drugs using the EC_{50}
365 value for [K^+]. In our experimental conditions, the EC_{50} value for [K^+] was about 10 mM (**Fig.**
366 **1 C**). The value is lower than that for skeletal muscle(Caputo and Bolanos, 1994) or
367 myotubes(Yang et al., 2006) in high [K^+]-induced Ca^{2+} transients. This may be partly explained
368 by measurement differences. We calculated the EC_{50} from the fluorescence intensity for 125–
369 150 seconds after stimulation (**Fig. 1 C**). This reduced the EC_{50} compared with the value
370 obtained just after stimulation in ER [Ca^{2+}] (**Fig. 1 C**) or cytoplasmic [Ca^{2+}] measurements (**Fig.**
371 **S3**). Nevertheless, our results reproduced the effects of disease-causing mutations (**Fig. 3–5**) or
372 drugs (**Fig. 6, 7**), strongly indicating that the EC_{50} value for [K^+] is a valid parameter for
373 quantitative evaluation.

374 Formation of DICR machinery can cause peripheral localization of the components, e.g.,
375 RyR1 and Cav1.1, in the reconstituted cells(Perni et al., 2017; Perni and Beam, 2022). In our
376 reconstituted cells, however, no such peripheral-specific localization was observed; the
377 components were localized throughout cells except for in nuclei (**Fig. S1**). This may be because
378 of high levels of the components expressed by baculovirus, which not only accelerates
379 formation of the DICR machinery (as discussed above), but also increases the number of
380 uncoupled components.

381 Mutations in Cav1.1 are implicated in various muscle diseases, including MH and
382 myopathy(Beam et al., 2017; Flucher, 2020). Among three MH mutations (R174W, R1086H
383 and T1354S), we demonstrated that R1086H, but not R174W orT1354S, significantly
384 accelerated DICR (**Fig. 4 C–E**). This is consistent with previous findings using Cav1.1-
385 deficient (dysgenic) myotubes (Weiss et al., 2004; Pirone et al., 2010; Eltit et al., 2012). All
386 three mutations show increased sensitivity to caffeine-induced Ca^{2+} release compared with WT,
387 indicating enhanced CICR activity (Weiss et al., 2004; Pirone et al., 2010; Eltit et al., 2012).
388 However, we showed that caffeine sensitivity was increased only for R1086H (**Fig. 4 F–H**). A
389 possible reason for this difference is the cells used. We used stable RyR1-overexpressing cells.
390 This may cause an excess amount of 'uncoupled' RyR1, which might mask the enhanced
391 sensitivity of caffeine dependence of the 'coupled' RyR1 by Cav1.1 mutations.

392 Most myopathy-related mutations identified in Cav1.1 have not been functionally
393 characterized. We evaluated four mutations (E100K, F275L, P742Q and L1367V) found in
394 patients with congenital myopathy(Schartner et al., 2017) (**Fig. 5**). We demonstrated that P742Q
395 substantially inhibited DICR with a large rightward shifted [K^+] dependence. This proline

396 resides in the II-III loop which interacts with RyR1 or Stac3(Wong King Yuen et al., 2017).
397 Substitution of the proline to threonine, the residue found in the corresponding position of
398 CaV1.2, diminished DICR in dysgenic myotubes(Kugler et al., 2004). Therefore, P742Q may
399 cause myopathy by reducing DICR activity. E100K and L1367V had no or only minor impacts
400 on DICR activity. These mutations might cause muscle weakness by reasons other than reduced
401 DICR. F275L is recessive because it was found in two compound heterozygous sisters carrying
402 F275L and the nonsense mutation, p.L791Cfs*37(Schartner et al., 2017). F275L completely
403 abolished DICR without any changes in ER [Ca^{2+}] or caffeine sensitivity. This does not fit with
404 a recessive mutation; if this is the case, patients will have no DICR activity. Further
405 investigations are required for this mutation.

406 There are no specific treatments for most DICR-related diseases; therefore, there is an
407 urgent need to develop novel drugs for these diseases(Agrawal et al., 2018; Flucher, 2020;
408 Lawal et al., 2020). We here evaluated DICR modulators. Among three known RyR1 inhibitors,
409 dantrolene and Cpd1 suppressed DICR (**Fig. 6**). This is consistent with the suppression of
410 twitch and tetanic tensions of isolated muscles and of reduced *in vivo* muscle weakness by
411 dantrolene(Meyler et al., 1979; Leslie and Part, 1981) and Cpd1(Yamazawa et al., 2021).
412 Interestingly, procaine did not suppress DICR (**Fig. 6**). Procaine inhibits CICR but not DICR
413 in frog skeletal muscle(Thorens and Endo, 1975) and reconstituted frog α-RyR and β-RyR in
414 RyR1-deficient myotubes(Kashiyama et al., 2010). Our data show similar procaine action in a
415 mammalian system. We also demonstrated that lyotropic anions (perchlorate and thiocyanate)
416 accelerate DICR (**Fig. 7**). This reproduces previous findings using skeletal muscle
417 fibers(Luttgau et al., 1983; Huang, 1986; Csernoch et al., 1987; Delay et al., 1990; Gonzalez
418 and Rios, 1993). Interestingly, lyotropic anions did not affect caffeine dependence, suggesting
419 no effect on CICR (**Fig. 7**). Therefore, our high-throughput platform will also be useful for drug
420 testing and screening for novel drugs that affect DICR.

421 In summary, we established a high-throughput platform for skeletal muscle DICR. This
422 platform is highly efficient and quantitative thus will be useful for both evaluation of disease-
423 causing mutations and the development of novel drugs for DICR-related diseases.

424

425 **Acknowledgments**

426 We thank Ikue Hiraga and the Laboratory of Proteomics and Biomolecular Science, Biomedical
427 Research Core Facilities, Juntendo University Graduate School of Medicine, for technical

assistance. We thank Jeremy Allen, PhD, from Edanz (https://jp.edanz.com/ac) for editing a draft of this manuscript. This work was supported by JSPS KAKENHI (19H03404 and 22H02805 to T.M., 19K07105 and 22K06652 to N.K., 20K11368 to T.K.), the Platform Project for Supporting Drug Discovery and Life Science Research (Basis for Supporting Innovative Drug Discovery and Life Science Research (BINDS)) from the Japan Agency for Medical Research and Development (AMED) (JP20am0101080 to T.M. and N.K. and JP20am0101098 to H.K.), an Intramural Research Grant for Neurological and Psychiatric Disorders from the National Center of Neurology and Psychiatry (2-5 to T.M.), the Vehicle Racing Commemorative Foundation (6237 and 6303 to T.M.), and the Cooperative Research Project of Research Center for Biomedical Engineering (to H.K.). The authors declare no competing financial interests.

Author contributions

T. Murayama, N. Kurebayashi, S. Okazaki, K. Yamashiro carried out the cell biological experiments; T. Numaga-Tomita and M. Yamada performed patch-clamp experiments; T. Nakada, S. Mori, R. Ishida, and H. Kagechika provided experimental tools; T. Murayama, N. Kurebayashi, T. Numaga-Tomita, T. Kobayashi, T. Nakada, M. Yamada, and T. Sakurai analyzed the experimental data; T. Murayama, N. Kurebayashi, T. Numaga-Tomita and M. Yamada wrote the manuscript. All authors reviewed and approved the manuscript.

448 **References**

449 Agrawal, A., G. Suryakumar, and R. Rathor. 2018. Role of defective Ca(2+) signaling in
450 skeletal muscle weakness: Pharmacological implications. *J Cell Commun Signal*.
451 12:645-659.

452 Beam, T.A., E.F. Loudermilk, and D.F. Kisor. 2017. Pharmacogenetics and pathophysiology of
453 CACNA1S mutations in malignant hyperthermia. *Physiol Genomics*. 49:81-87.

454 Block, B.A., T. Imagawa, K.P. Campbell, and C. Franzini-Armstrong. 1988. Structural evidence
455 for direct interaction between the molecular components of the transverse
456 tubule/sarcoplasmic reticulum junction in skeletal muscle. *J Cell Biol*. 107:2587-2600.

457 Caputo, C., and P. Bolanos. 1994. Fluo-3 signals associated with potassium contractures in
458 single amphibian muscle fibres. *J Physiol*. 481 (Pt 1):119-128.

459 Carpenter, D., C. Ringrose, V. Leo, A. Morris, R.L. Robinson, P.J. Halsall, P.M. Hopkins, and
460 M.A. Shaw. 2009. The role of CACNA1S in predisposition to malignant hyperthermia.
461 *BMC Med Genet*. 10:104.

462 Catterall, W.A. 2000. Structure and regulation of voltage-gated Ca2+ channels. *Annu Rev Cell*
463 *Dev Biol*. 16:521-555.

464 Csernoch, L., L. Kovacs, and G. Szucs. 1987. Perchlorate and the relationship between charge
465 movement and contractile activation in frog skeletal muscle fibres. *J Physiol*. 390:213-
466 227.

467 Delay, M., D.E. Garcia, and J.A. Sanchez. 1990. The effects of lyotropic anions on charge
468 movement, calcium currents and calcium signals in frog skeletal muscle fibres. *J*
469 *Physiol*. 425:449-469.

470 DiFranco, M., C. Yu, M. Quinonez, and J.L. Vergara. 2015. Inward rectifier potassium currents
471 in mammalian skeletal muscle fibres. *J Physiol*. 593:1213-1238.

472 Eltit, J.M., R.A. Bannister, O. Moua, F. Altamirano, P.M. Hopkins, I.N. Pessah, T.F. Molinski,
473 J.R. Lopez, K.G. Beam, and P.D. Allen. 2012. Malignant hyperthermia susceptibility
474 arising from altered resting coupling between the skeletal muscle L-type Ca2+ channel
475 and the type 1 ryanodine receptor. *Proc Natl Acad Sci U S A*. 109:7923-7928.

476 Flucher, B.E. 2020. Skeletal muscle CaV1.1 channelopathies. *Pflugers Arch*. 472:739-754.

477 Flucher, B.E., and M. Campiglio. 2019. STAC proteins: The missing link in skeletal muscle EC
478 coupling and new regulators of calcium channel function. *Biochim Biophys Acta Mol*
479 *Cell Res*. 1866:1101-1110.

480 Flucher, B.E., G.J. Obermair, P. Tuluc, J. Schredelseker, G. Kern, and M. Grabner. 2005. The
481 role of auxiliary dihydropyridine receptor subunits in muscle. *J Muscle Res Cell Motil*.
482 26:1-6.

483 Franzini-Armstrong, C. 2018. The relationship between form and function throughout the
484 history of excitation-contraction coupling. *J Gen Physiol*. 150:189-210.

485 Gonzalez, A., and E. Rios. 1993. Perchlorate enhances transmission in skeletal muscle
486 excitation-contraction coupling. *J Gen Physiol*. 102:373-421.

487 Gregg, R.G., A. Messing, C. Strube, M. Beurg, R. Moss, M. Behan, M. Sukhareva, S. Haynes,
488 J.A. Powell, R. Coronado, and P.A. Powers. 1996. Absence of the beta subunit (cchb1)
489 of the skeletal muscle dihydropyridine receptor alters expression of the alpha 1 subunit
490 and eliminates excitation-contraction coupling. *Proc Natl Acad Sci U S A*. 93:13961-
491 13966.

492 Horstick, E.J., J.W. Linsley, J.J. Dowling, M.A. Hauser, K.K. McDonald, A. Ashley-Koch, L.
493 Saint-Amant, A. Satish, W.W. Cui, W. Zhou, S.M. Sprague, D.S. Stamm, C.M. Powell,
494 M.C. Speer, C. Franzini-Armstrong, H. Hirata, and J.Y. Kuwada. 2013. Stac3 is a
495 component of the excitation-contraction coupling machinery and mutated in Native
496 American myopathy. *Nat Commun*. 4:1952.

497 Huang, C.L. 1986. The differential effects of twitch potentiators on charge movements in frog
498 skeletal muscle. *J Physiol*. 380:17-33.

499 Kashiyama, T., T. Murayama, E. Suzuki, P.D. Allen, and Y. Ogawa. 2010. Frog alpha- and beta-
500 ryanodine receptors provide distinct intracellular Ca2+ signals in a myogenic cell line.
501 *PLoS One*. 5:e11526.

502 Kirkton, R.D., and N. Bursac. 2011. Engineering biosynthetic excitable tissues from
503 unexcitable cells for electrophysiological and cell therapy studies. *Nat Commun*. 2:300.

504 Kitts, P.A., and G. Green. 1999. An immunological assay for determination of baculovirus titers
505 in 48 hours. *Anal Biochem*. 268:173-178.

506 Kugler, G., R.G. Weiss, B.E. Flucher, and M. Grabner. 2004. Structural requirements of the
507 dihydropyridine receptor alpha1S II-III loop for skeletal-type excitation-contraction
508 coupling. *J Biol Chem*. 279:4721-4728.

509 Lawal, T.A., J.J. Todd, J.W. Witherspoon, C.G. Bonnemann, J.J. Dowling, S.L. Hamilton, K.G.
510 Meilleur, and R.T. Dirksen. 2020. Ryanodine receptor 1-related disorders: an historical
511 perspective and proposal for a unified nomenclature. *Skelet Muscle*. 10:32.

512 Leslie, G.C., and N.J. Part. 1981. The action of dantrolene sodium on rat fast and slow muscle
513 in vivo. *Br J Pharmacol*. 72:665-672.

514 Luttgau, H.C., G. Gottschalk, L. Kovacs, and M. Fuxreiter. 1983. How perchlorate improves
515 excitation-contraction coupling in skeletal muscle fibers. *Biophys J*. 43:247-249.

516 Meyler, W.J., I. Mols-Thurkow, A.H. Scaf, S. Sargo, and H. Wesseling. 1979. The effect of
517 dantrolene sodium on rat skeletal muscle in relation to the plasma concentration. *Eur J*
518 *Pharmacol*. 53:335-342.

519 Mori, S., H. Iinuma, N. Manaka, M. Ishigami-Yuasa, T. Murayama, Y. Nishijima, A. Sakurai,
520 R. Arai, N. Kurebayashi, T. Sakurai, and H. Kagechika. 2019. Structural development
521 of a type-1 ryanodine receptor (RyR1) Ca(2+)-release channel inhibitor guided by
522 endoplasmic reticulum Ca(2+) assay. *Eur J Med Chem*. 179:837-848.

523 Murayama, T., and N. Kurebayashi. 2019. Assays for Modulators of Ryanodine Receptor
524 (RyR)/Ca(2+) Release Channel Activity for Drug Discovery for Skeletal Muscle and
525 Heart Diseases. *Curr Protoc Pharmacol*. 87:e71.

526 Murayama, T., N. Kurebayashi, M. Ishigami-Yuasa, S. Mori, Y. Suzuki, R. Akima, H. Ogawa,
527 J. Suzuki, K. Kanemaru, H. Oyamada, Y. Kiuchi, M. Iino, H. Kagechika, and T. Sakurai.
528 2018. Efficient High-Throughput Screening by Endoplasmic Reticulum Ca^{2+}
529 Measurement to Identify Inhibitors of Ryanodine Receptor Ca^{2+}-Release Channels. *Mol*
530 *Pharmacol*. 94:722-730.

531 Murayama, T., N. Kurebayashi, T. Yamazawa, H. Oyamada, J. Suzuki, K. Kanemaru, K. Oguchi,
532 M. Iino, and T. Sakurai. 2015. Divergent Activity Profiles of Type 1 Ryanodine Receptor
533 Channels Carrying Malignant Hyperthermia and Central Core Disease Mutations in the
534 Amino-Terminal Region. *PLoS One*. 10:e0130606.

535 Nelson, B.R., F. Wu, Y. Liu, D.M. Anderson, J. McAnally, W. Lin, S.C. Cannon, R. Bassel-
536 Duby, and E.N. Olson. 2013. Skeletal muscle-specific T-tubule protein STAC3 mediates
537 voltage-induced Ca2+ release and contractility. *Proc Natl Acad Sci U S A*. 110:11881-
538 11886.

539 Obermair, G.J., G. Kugler, S. Baumgartner, P. Tuluc, M. Grabner, and B.E. Flucher. 2005. The
540 Ca2+ channel alpha2delta-1 subunit determines Ca2+ current kinetics in skeletal muscle
541 but not targeting of alpha1S or excitation-contraction coupling. *J Biol Chem*. 280:2229-
542 2237.

543 Perez, C.F., J.M. Eltit, J.R. Lopez, D. Bodnar, A.F. Dulhunty, S. Aditya, and M.G. Casarotto.
544 2018. Functional and structural characterization of a novel malignant hyperthermia-

susceptible variant of DHPR-beta1a subunit (CACNB1). *Am J Physiol Cell Physiol*. 314:C323-C333.

Perni, S., and K. Beam. 2022. Junctophilins 1, 2, and 3 all support voltage-induced Ca2+ release despite considerable divergence. *J Gen Physiol*. 154.

Perni, S., M. Lavorato, and K.G. Beam. 2017. De novo reconstitution reveals the proteins required for skeletal muscle voltage-induced Ca(2+) release. *Proc Natl Acad Sci U S A*. 114:13822-13827.

Pirone, A., J. Schredelseker, P. Tuluc, E. Gravino, G. Fortunato, B.E. Flucher, A. Carsana, F. Salvatore, and M. Grabner. 2010. Identification and functional characterization of malignant hyperthermia mutation T1354S in the outer pore of the Cavalpha1S-subunit. *Am J Physiol Cell Physiol*. 299:C1345-1354.

Polster, A., B.R. Nelson, E.N. Olson, and K.G. Beam. 2016. Stac3 has a direct role in skeletal muscle-type excitation-contraction coupling that is disrupted by a myopathy-causing mutation. *Proc Natl Acad Sci U S A*. 113:10986-10991.

Reinholt, B.M., X. Ge, X. Cong, D.E. Gerrard, and H. Jiang. 2013. Stac3 is a novel regulator of skeletal muscle development in mice. *PLoS One*. 8:e62760.

Riazi, S., N. Kraeva, and P.M. Hopkins. 2018. Updated guide for the management of malignant hyperthermia. *Can J Anaesth*. 65:709-721.

Rios, E., and G. Pizarro. 1991. Voltage sensor of excitation-contraction coupling in skeletal muscle. *Physiol Rev*. 71:849-908.

Rufenach, B., and F. Van Petegem. 2021. Structure and function of STAC proteins: Calcium channel modulators and critical components of muscle excitation-contraction coupling. *J Biol Chem*. 297:100874.

Schartner, V., N.B. Romero, S. Donkervoort, S. Treves, P. Munot, T.M. Pierson, I. Dabaj, E. Malfatti, I.T. Zaharieva, F. Zorzato, O. Abath Neto, G. Brochier, X. Lornage, B. Eymard, A.L. Taratuto, J. Bohm, H. Gonorazky, L. Ramos-Platt, L. Feng, R. Phadke, D.X. Bharucha-Goebel, C.J. Sumner, M.T. Bui, E. Lacene, M. Beuvin, C. Labasse, N. Dondaine, R. Schneider, J. Thompson, A. Boland, J.F. Deleuze, E. Matthews, A.N. Pakleza, C.A. Sewry, V. Biancalana, S. Quijano-Roy, F. Muntoni, M. Fardeau, C.G. Bonnemann, and J. Laporte. 2017. Dihydropyridine receptor (DHPR, CACNA1S) congenital myopathy. *Acta Neuropathol*. 133:517-533.

Schneider, M.F. 1994. Control of calcium release in functioning skeletal muscle fibers. *Annu*

Rev Physiol. 56:463-484.

Schredelseker, J., M. Shrivastav, A. Dayal, and M. Grabner. 2010. Non-Ca2+-conducting Ca2+ channels in fish skeletal muscle excitation-contraction coupling. *Proc Natl Acad Sci U S A*. 107:5658-5663.

Shishmarev, D. 2020. Excitation-contraction coupling in skeletal muscle: recent progress and unanswered questions. *Biophys Rev*. 12:143-153.

Stewart, S.L., K. Hogan, H. Rosenberg, and J.E. Fletcher. 2001. Identification of the Arg1086His mutation in the alpha subunit of the voltage-dependent calcium channel (CACNA1S) in a North American family with malignant hyperthermia. *Clin Genet*. 59:178-184.

Suzuki, J., K. Kanemaru, K. Ishii, M. Ohkura, Y. Okubo, and M. Iino. 2014. Imaging intraorganellar Ca2+ at subcellular resolution using CEPIA. *Nat Commun*. 5:4153.

Takeshima, H., M. Iino, H. Takekura, M. Nishi, J. Kuno, O. Minowa, H. Takano, and T. Noda. 1994. Excitation-contraction uncoupling and muscular degeneration in mice lacking functional skeletal muscle ryanodine-receptor gene. *Nature*. 369:556-559.

Takeshima, H., S. Komazaki, M. Nishi, M. Iino, and K. Kangawa. 2000. Junctophilins: a novel family of junctional membrane complex proteins. *Mol Cell*. 6:11-22.

Tanabe, T., K.G. Beam, J.A. Powell, and S. Numa. 1988. Restoration of excitation-contraction coupling and slow calcium current in dysgenic muscle by dihydropyridine receptor complementary DNA. *Nature*. 336:134-139.

Tani, H., M. Nishijima, H. Ushijima, T. Miyamura, and Y. Matsuura. 2001. Characterization of cell-surface determinants important for baculovirus infection. *Virology*. 279:343-353.

Thorens, S., and M. Endo. 1975. Calcium-induced calcium release and “depolarization”-induced calcium release: their physiological significance. *Proc Jpn Acad*. 51:473-478.

Tong, J., H. Oyamada, N. Demaurex, S. Grinstein, T.V. McCarthy, and D.H. MacLennan. 1997. Caffeine and halothane sensitivity of intracellular Ca2+ release is altered by 15 calcium release channel (ryanodine receptor) mutations associated with malignant hyperthermia and/or central core disease. *J Biol Chem*. 272:26332-26339.

Uehara, A., T. Murayama, M. Yasukochi, M. Fill, M. Horie, T. Okamoto, Y. Matsuura, K. Uehara, T. Fujimoto, T. Sakurai, and N. Kurebayashi. 2017. Extensive Ca2+ leak through K4750Q cardiac ryanodine receptors caused by cytosolic and luminal Ca2+ hypersensitivity. *J Gen Physiol*. 149:199-218.

Ursu, D., R.P. Schuhmeier, M. Freichel, V. Flockerzi, and W. Melzer. 2004. Altered inactivation of Ca2+ current and Ca2+ release in mouse muscle fibers deficient in the DHP receptor gamma1 subunit. *J Gen Physiol*. 124:605-618.

Weiss, R.G., K.M. O'Connell, B.E. Flucher, P.D. Allen, M. Grabner, and R.T. Dirksen. 2004. Functional analysis of the R1086H malignant hyperthermia mutation in the DHPR reveals an unexpected influence of the III-IV loop on skeletal muscle EC coupling. *Am J Physiol Cell Physiol*. 287:C1094-1102.

Wong King Yuen, S.M., M. Campiglio, C.C. Tung, B.E. Flucher, and F. Van Petegem. 2017. Structural insights into binding of STAC proteins to voltage-gated calcium channels. *Proc Natl Acad Sci U S A*. 114:E9520-E9528.

Yamazawa, T., T. Kobayashi, N. Kurebayashi, M. Konishi, S. Noguchi, T. Inoue, Y.U. Inoue, I. Nishino, S. Mori, H. Iinuma, N. Manaka, H. Kagechika, A. Uryash, J. Adams, J.R. Lopez, X. Liu, C. Diggle, P.D. Allen, S. Kakizawa, K. Ikeda, B. Lin, Y. Ikemi, K. Nunomura, S. Nakagawa, T. Sakurai, and T. Murayama. 2021. A novel RyR1-selective inhibitor prevents and rescues sudden death in mouse models of malignant hyperthermia and heat stroke. *Nat Commun*. 12:4293.

Yang, T., J. Riehl, E. Esteve, K.I. Matthaei, S. Goth, P.D. Allen, I.N. Pessah, and J.R. Lopez. 2006. Pharmacologic and functional characterization of malignant hyperthermia in the R163C RyR1 knock-in mouse. *Anesthesiology*. 105:1164-1175.

Zhao, Y., S. Araki, J. Wu, T. Teramoto, Y.F. Chang, M. Nakano, A.S. Abdelfattah, M. Fujiwara, T. Ishihara, T. Nagai, and R.E. Campbell. 2011. An expanded palette of genetically encoded Ca(2)(+) indicators. *Science*. 333:1888-1891.

633 **Figure legends**

634 Figure 1 **DICR measurements in 96-well plates using a fluorescence microplate reader. (A)**
635 Schematic drawing of RyR1/R-CEPIA1er HEK293 cells without (No BV, left) and with (5 BV,
636 right) baculovirus infection of essential components for DICR (Cav1.1, β1a, JP2, Stac3) and
637 Kir2.1. **(B)** Typical results of time-lapse R-CEPIA1er fluorescence measurement using a
638 FlexStation3 fluorescence microplate reader for RyR1/R-CEPIA1er HEK293 cells without (left,
639 No BV) or with (right, 5 BV) BV infection. High [K^+] solution ranging from 5–61 mM (symbols
640 shown in right) or 10 mM caffeine (light blue) was applied at 30 seconds after starting (blue
641 arrowheads). **(C)** [K^+] dependence of R-CEPIA1er fluorescence (F/F_0) in No BV (black) and 5
642 BV cells (red). F/F_0 was obtained by normalizing the fluorescence (F) at 35 sec (open circles)
643 or the averaged fluorescence of 125-150 sec to that of the first 25 seconds (F_0). Data are means
644 ± SD (n = 6). Note that [K^+] dependent plot with data at 35 sec (open red) was shifted
645 rightward compared with that from data at 125–150 sec (filled red) with larger variations,
646 especially around EC_{50} values. **(D)** Fluorescence change by 61 mM [K^+] or 10 mM caffeine.
647 Fluorescence change is expressed as $1-F/F_0$ (see panel **C**). Data are means ± SD (n = 6) and
648 were analyzed by two-way ANOVA with Bonferroni's multiple comparisons test. Note that 5
649 BV cells show large fluorescence change with high [K^+] which is nearly 80% of that with
650 caffeine.

651

652 Figure 2 **Validation of the reconstituted DICR platform. (A)** Typical results of R-CEPIA1er
653 fluorescence in cells infected with 5 BV (left), BV without Cav1.1 (center), and 5 BV plus γ1
654 (right). (**B**) [K^+] dependence of R-CEPIA1er fluorescence (F/F_0) in 5 BV (black), -Cav1.1 (red),
655 and -JP2 (dark blue). Data are means ± SD (n = 9 for 5 BV, 6 for -Cav1.1 and -JP2). **(C)**
656 Fluorescence change by 61 mM [K^+] in the BV-infected cells lacking one of essential
657 components (-Cav1.1, -β1a, -Stac3, or -JP2) or with RyR2 cells instead of RyR1. Data are
658 means ± SD (n = 6) and were analyzed by one-way ANOVA with Dunnett's multiple
659 comparisons test. **(D)** [K^+] dependence of R-CEPIA1er fluorescence (F/F_0) in cells infected
660 with 5 BV (black), 5 BV plus α_2-δ (purple) and 5 BV plus γ1 (orange). Data are means ± SD (n
661 = 6). **(E)** Fluorescence change by 61 mM [K^+] in 5 BV, +α_2-δ, and +γ1 cells. Data are means ±
662 SD (n = 6) and were analyzed by one-way ANOVA with Dunnett's multiple comparisons test.

663

664 Figure 3 **Importance of Kir2.1 on DICR platform. (A)** Resting membrane potential of cells
665 infected with 5 BV (left) or BV without Kir2.1 (-Kir2.1) (right). Data are means ± SD (n = 10

666 and 16 for 5 mM and 50 mM [K^+], respectively, for 5 BV and 10 and 14 for 5 mM and 50 mM
667 [K^+], respectively, for -Kir2.1) and were analyzed by two-way ANOVA with Bonferroni's
668 multiple comparisons test. **(B)** Typical results of R-CEPIA1er fluorescence in cells infected
669 with 5 BV (left) and BV without Kir2.1 (right). High [K^+] solution ranging from 5–61 mM
670 (symbols shown in left) was applied at 30 seconds after starting (blue arrowheads). **(C)** Typical
671 results of ER [Ca^{2+}] measurement in cells with 5 BV (left), without Kir2.1, without Kir2.1 and
672 β1a, and without Kir2.1 and Stac3. **(D)** Resting ER [Ca^{2+}] in cells infected with 5 BV, BV
673 without Kir2.1 (-Kir2.1), Kir2.1 and β1a (-Kir2.1, -β1a), or Kir2.1 and Stac3 (-Kir2.1, -Stac3).
674 Data are means ± SD (n = 8) and were analyzed by one-way ANOVA with Dunnett's multiple
675 comparisons test.
676
677 Figure 4 **Effect of MH mutations in Cav1.1 on DICR activity. (A)** Schematic drawing of the
678 location of MH mutations (R174W, R1086H and T1354S) in Cav1.1. **(B)** Resting ER [Ca^{2+}] in
679 cells expressing WT and mutant Cav1.1. Data are means ± SD (n = 12) and were analyzed by
680 one-way ANOVA with Dunnett's multiple comparisons test. **(C)** [K^+] dependence of R-
681 CEPIA1er fluorescence (F/F_0) in WT (black), R174W (red), R1086H (blue) and T1354S
682 (green) Cav1.1 cells. Data are means ± SD (n = 9). **(D, E)** Fluorescence change by 61 mM [K^+]
683 (**D**) and EC_{50} values for [K^+] (**E**). Data are means ± SD (n = 9) and were analyzed by one-way
684 ANOVA with Dunnett's multiple comparisons test. **(F)** Caffeine dependence of v(F/F_0) in WT
685 (black), R174W (red), R1086H (blue) and T1354S (green) Cav1.1 cells. Data are means ± SD
686 (n = 9). **(G, H)** Fluorescence change by 20 mM caffeine (**G**) and EC_{50} values for caffeine (**H**).
687 Data are means ± SD (n = 9) and were analyzed by one-way ANOVA with Dunnett's multiple
688 comparisons test.
689
690 Figure 5 **Effect of myopathy mutations in Cav1.1 on DICR activity. (A)** Schematic drawing
691 of the location of myopathy mutations (E100K, F275L, P742Q and L1367V) in Cav1.1. **(B)**
692 Resting ER [Ca^{2+}] in cells expressing WT and mutant Cav1.1. Data are means ± SD (n = 12)
693 and were analyzed by one-way ANOVA with Dunnett's multiple comparisons test. **(C)** [K^+]
694 dependence of R-CEPIA1er fluorescence (F/F_0) in WT (black), E100K (red), F275L (blue),
695 P742Q (green) and L1367V (magenta) Cav1.1 cells. Data are means ± SD (n = 9). **(D, E)**
696 Fluorescence change by 61 mM [K^+] (**D**) and EC_{50} values for [K^+] (**E**). Data are means ± SD
697 (n = 9) and were analyzed by one-way ANOVA with Dunnett's multiple comparisons test. **(F)**
698 Caffeine dependence of R-CEPIA1er fluorescence (F/F_0) in WT (black), E100K (red), F275L

699 (blue), P742Q (green) and L1367V (magenta) Cav1.1 cells. Data are means ± SD (n = 9). **(G,**
700 **H)** Fluorescence change by 20 mM caffeine (**G**) and EC_{50} values for caffeine (**H**). Data are
701 means ± SD (n = 9) and were analyzed by one-way ANOVA with Dunnett's multiple
702 comparisons test.
703
704 Figure 6 **Effect of RyR1 inhibitors on DICR activity. (A)** Chemical structures of dantrolene,
705 Cpd1 and procaine. **(B)** $[K^+]$ dependence of fluorescence change (F/F_0) in cells without (Control,
706 black) or with dantrolene (10 μM, red), Cpd1 (3 μM, blue) or procaine (5 mM, green). Data are
707 means ± SD (n = 9). **(C)** EC_{50} values for $[K^+]$. Data are means ± SD (n = 9) and were analyzed
708 by one-way ANOVA with Dunnett's multiple comparisons test. **(D)** Caffeine dependence of R-
709 CEPIA1er fluorescence (F/F_0) in cells without (Control, black) or with dantrolene (10 μM, red),
710 Cpd1 (3 μM, blue) or procaine (5 mM, green). Data are means ± SD (n = 9). **(E)** EC_{50} values
711 for caffeine. Data are means ± SD (n = 9) and were analyzed by one-way ANOVA with
712 Dunnett's multiple comparisons test.
713
714 Figure 7 **Effect of lyotropic anions on DICR activity. (A)** $[K^+]$ dependence of fluorescence
715 change (F/F_0) in cells in the absence (Control, black) or presence of perchlorate (10 mM, red)
716 or thiocyanate (10 mM, blue). Data are means ± SD (n = 9). **(B)** EC_{50} values for $[K^+]$. Data are
717 means ± SD (n = 9) and were analyzed by one-way ANOVA with Dunnett's multiple
718 comparisons test. **(C)** Caffeine dependence of R-CEPIA1er fluorescence (F/F_0) in cells in the
719 absence (Control, black) or presence of perchlorate (10 mM, red) or thiocyanate (10 mM, blue).
720 Data are means ± SD (n = 9). **(D)** EC_{50} values for caffeine. Data are means ± SD (n = 9) and
721 were analyzed by one-way ANOVA with Dunnett's multiple comparisons test.
722
723

Table 1. List of PCR primers.

mCav1.1-F, AAAAAGCTTGCCACCATGGAGCCGCCCTCACCCCAG

mCav1.1-R, TTTACGCGTTCAAGGCTCCCAGGGCACGGC

mβ1a-F, AAAGCTAGCCACCATGGTCCAGAAGAGCGGCATG

mβ1a-R, TTTGATATCCTACATGGCGTGCTCCTGAGG

mJP2-F, AAAGCTAGCCACCATGAGCGGGGGCCGCTTTGAC

mJP2-R, TTTGATATCTCAAGTCAGGAGGTGAACAAA

mStac3-F, AAAGCTAGCCACCATGACAGAAAAGGAAGTGGTG

mStac3-R, TTTACGCGTTTAAATCTCCTCCAGGAAGTC

mKir2.1-F, AAAGCTAGCCACCATGGGCAGTGTGAGAACCAAC

mKir2.1-R, TTTACGCGTTCATATCTCCGATTCTCGCCT

rα2δ-F, AAAGCTAGCCACCATGGCTGCTGGCTGCCTGCTG

rα2δ-R, TTTACGCGTTCACCATAGATAGTGTCTGCT

mγ1-F, AAAGCTAGCCACCATGTCACAGACCAAAACAGCG

mγ1-R, TTTACGCGTCTAGTGCTCTGGCTCAGCGTC

Figure 1

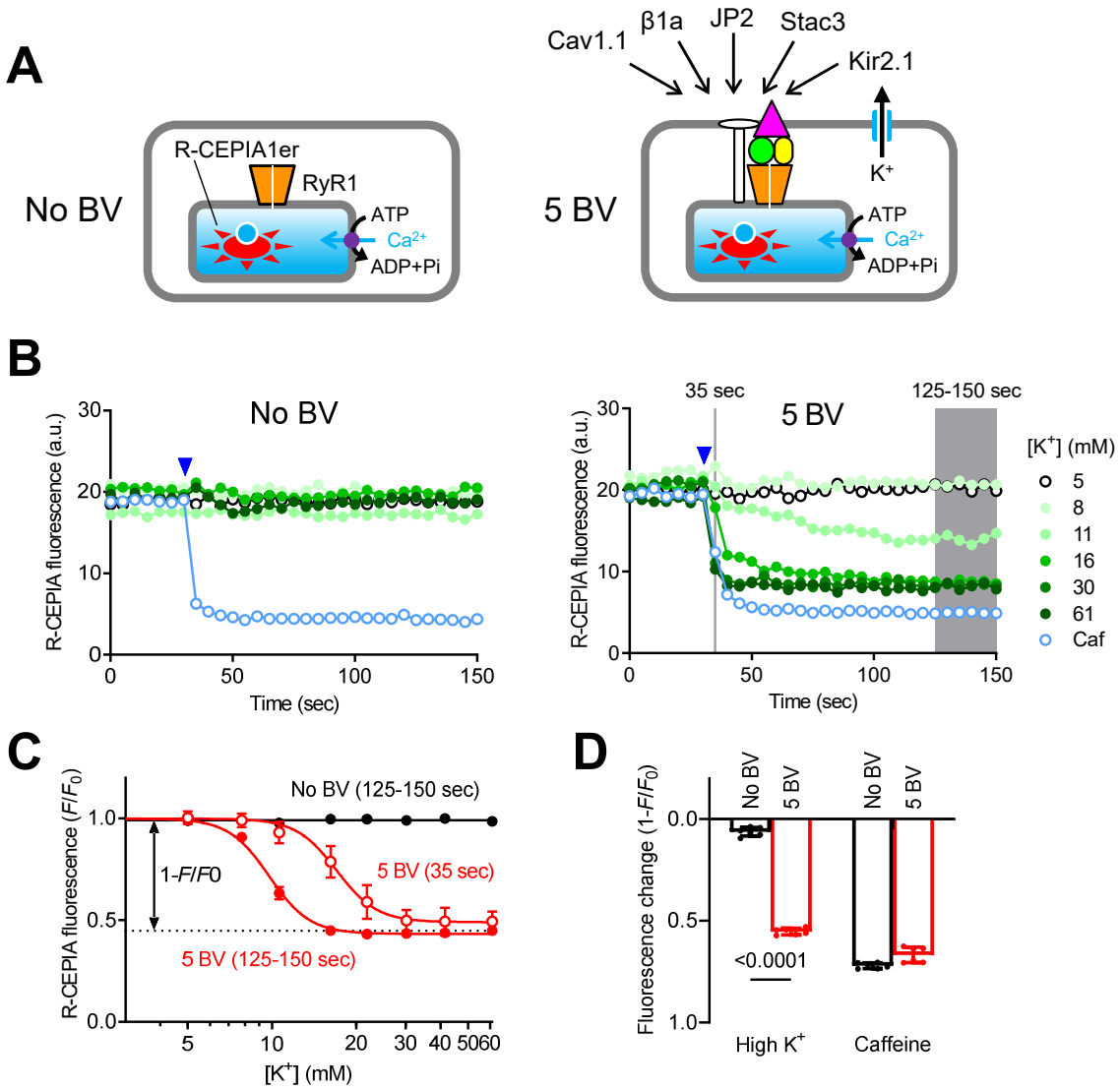

Figure 1 **DICR measurements in 96-well plates using a fluorescence microplate reader. (A)** Schematic drawing of RyR1/R-CEPIA1er HEK293 cells without (No BV, left) and with (5 BV, right) baculovirus infection of essential components for DICR (Cav1.1, β1a, JP2, Stac3) and Kir2.1. **(B)** Typical results of time-lapse R-CEPIA1er fluorescence measurement using a FlexStation3 fluorescence microplate reader for RyR1/R-CEPIA1er HEK293 cells without (left, No BV) or with (right, 5 BV) BV infection. High [K^+] solution ranging from 5–61 mM (symbols shown in right) or 10 mM caffeine (light blue) was applied at 30 seconds after starting (blue arrowheads). **(C)** [K^+] dependence of R-CEPIA1er fluorescence (F/F_0) in No BV (black) and 5 BV cells (red). F/F_0 was obtained by normalizing the fluorescence (F) at 35 sec (open circles) or the averaged fluorescence of 125-150 sec to that of the first 25 seconds (F_0). Data are means ± SD (n = 6). Note that [K^+] dependent plot with data at 35 sec (open red) was shifted rightward compared with that from data at 125–150 sec (filled red) with larger variations, especially around EC_{50} values. **(D)** Fluorescence change by 61 mM [K^+] or 10 mM caffeine. Fluorescence change is expressed as $1\text{-}F/F_0$ (see panel **C**). Data are means ± SD (n = 6) and were analyzed by two-way ANOVA with Bonferroni's multiple comparisons test. Note that 5 BV cells show large fluorescence change with high [K^+] which is nearly 80% of that with caffeine.

Figure 2

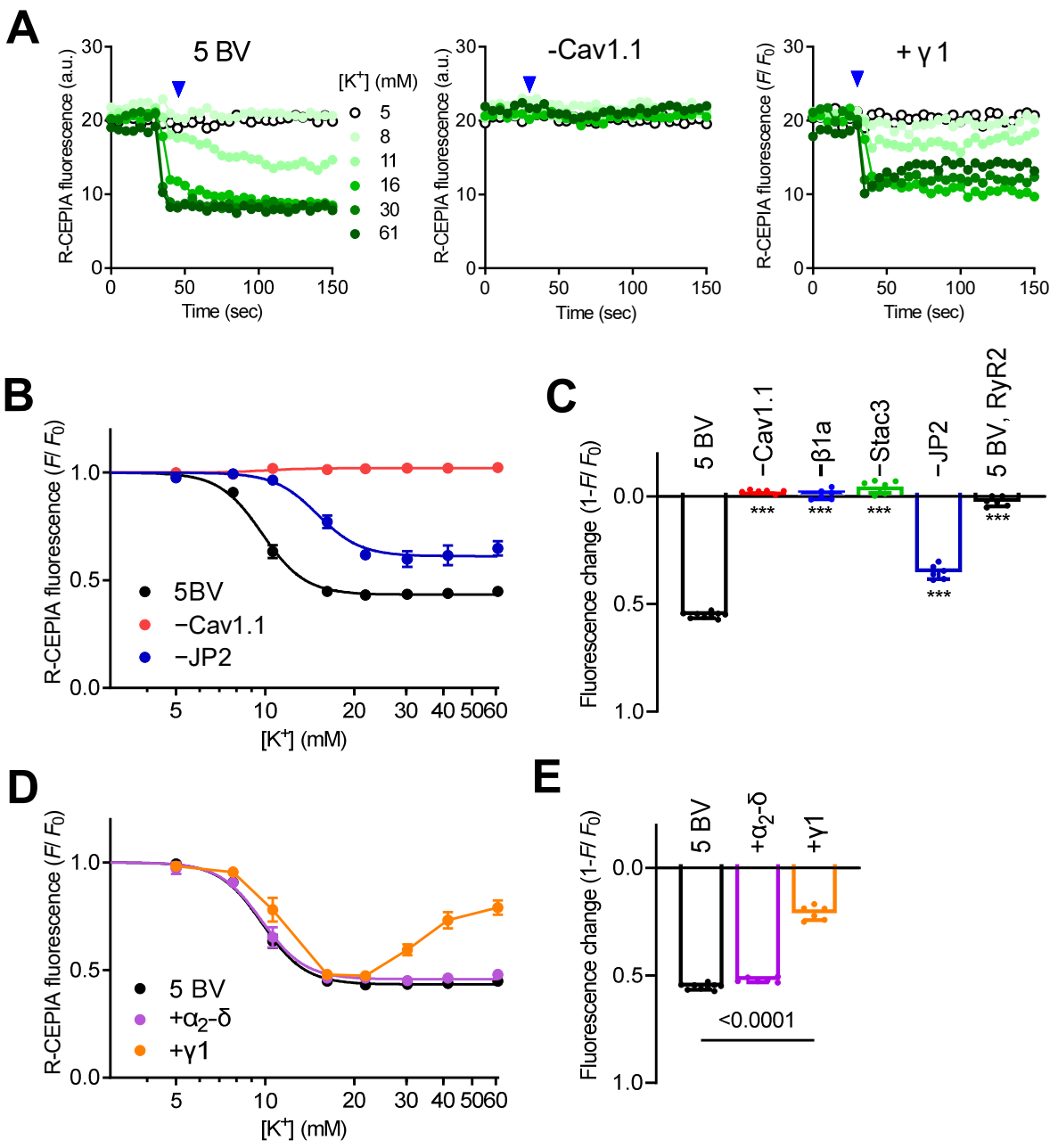

Figure 2 **Validation of the reconstituted DICR platform. (A)** Typical results of R-CEPIA1er fluorescence in cells infected with 5 BV (left), BV without Cav1.1 (center), and 5 BV plus γ1 (right). (**B**) [K^+] dependence of R-CEPIA1er fluorescence (F/F_0) in 5 BV (black), -Cav1.1 (red), and -JP2 (dark blue). Data are means ± SD (n = 9 for 5 BV, 6 for -Cav1.1 and -JP2). **(C)** Fluorescence change by 61 mM [K^+] in the BV-infected cells lacking one of essential components (-Cav1.1, -β1a, -Stac3, or -JP2) or with RyR2 cells instead of RyR1. Data are means ± SD (n = 6) and were analyzed by one-way ANOVA with Dunnett's multiple comparisons test. **(D)** [K^+] dependence of R-CEPIA1er fluorescence (F/F_0) in cells infected with 5 BV (black), 5 BV plus α_2-δ (+α_2-δ, purple) and 5 BV plus γ1 (+γ1, orange). Data are means ± SD (n = 6). **(E)** Fluorescence change by 61 mM [K^+] in 5 BV, +α_2-δ, and +γ1 cells. Data are means ± SD (n = 6) and were analyzed by one-way ANOVA with Dunnett's multiple comparisons test.

Figure 3

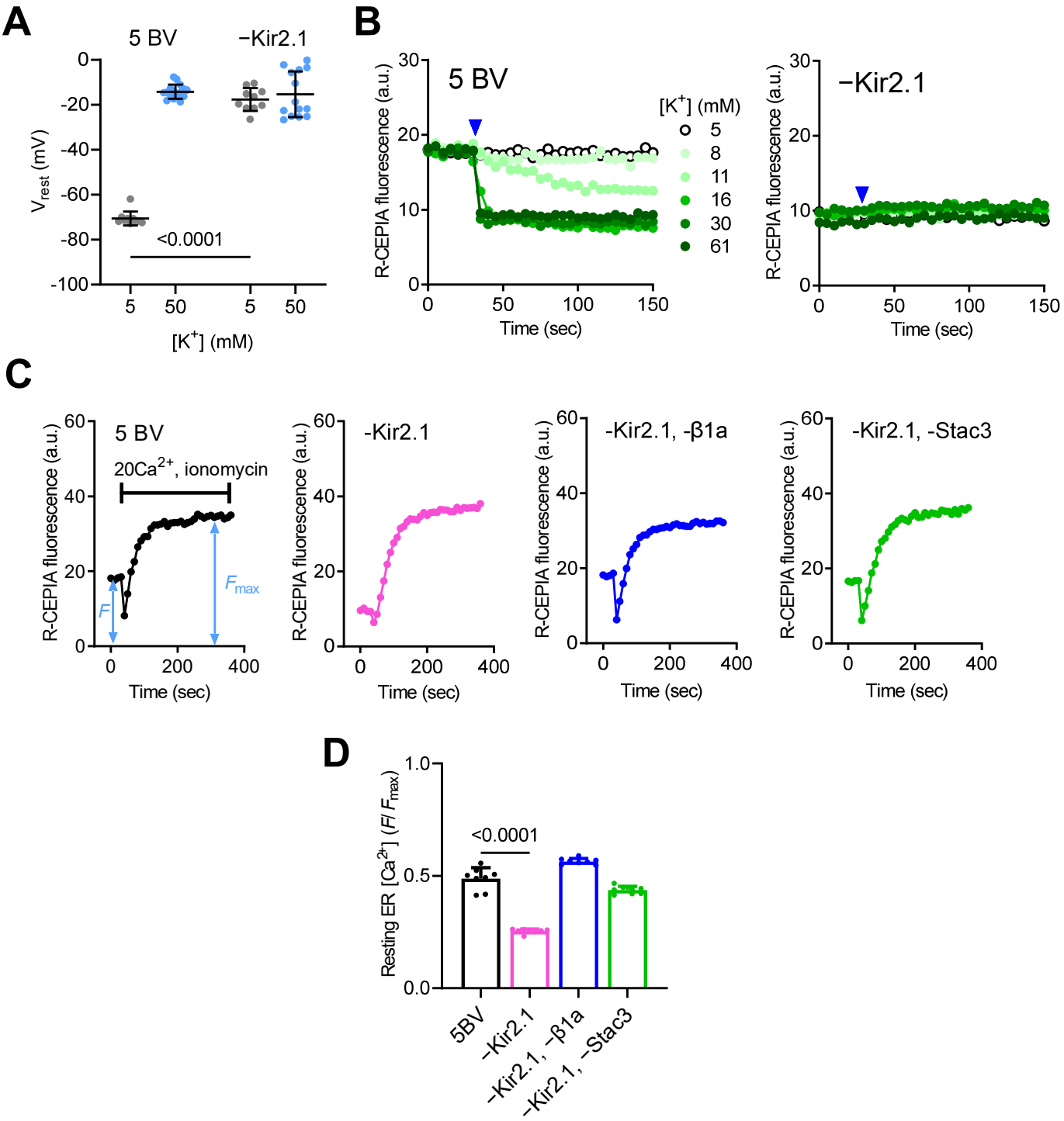

Figure 3 **Importance of Kir2.1 on DICR platform. (A)** Membrane potential of cells infected with 5 BV (left) or BV without Kir2.1 (-Kir2.1) (right). Data are means ± SD (n = 10 and 16 for 5 mM and 50 mM K^+, respectively, for 5 BV and 10 and 14 for 5 mM and 50 mM K^+, respectively, for -Kir2.1) and were analyzed by two-way ANOVA with Bonferroni's multiple comparisons test. **(B)** Typical results of R-CEPIA1er fluorescence in cells infected with 5 BV (left) and BV without Kir2.1 (right). High [K^+] solution ranging from 5–61 mM (symbols shown in left) was applied at 30 seconds after starting (blue arrowheads). **(C)** Typical results of ER [Ca^{2+}] measurement in cells with 5 BV, without Kir2.1, without Kir2.1 and β1a, and without Kir2.1 and Stac3. **(D)** Resting ER [Ca^{2+}] in cells infected with 5 BV, BV without Kir2.1 (-Kir2.1), Kir2.1 and β1a (-Kir2.1, -β1a), or Kir2.1 and Stac3 (-Kir2.1, -Stac3). Data are means ± SD (n = 8) and were analyzed by one-way ANOVA with Dunnett's multiple comparisons test.

Figure 4

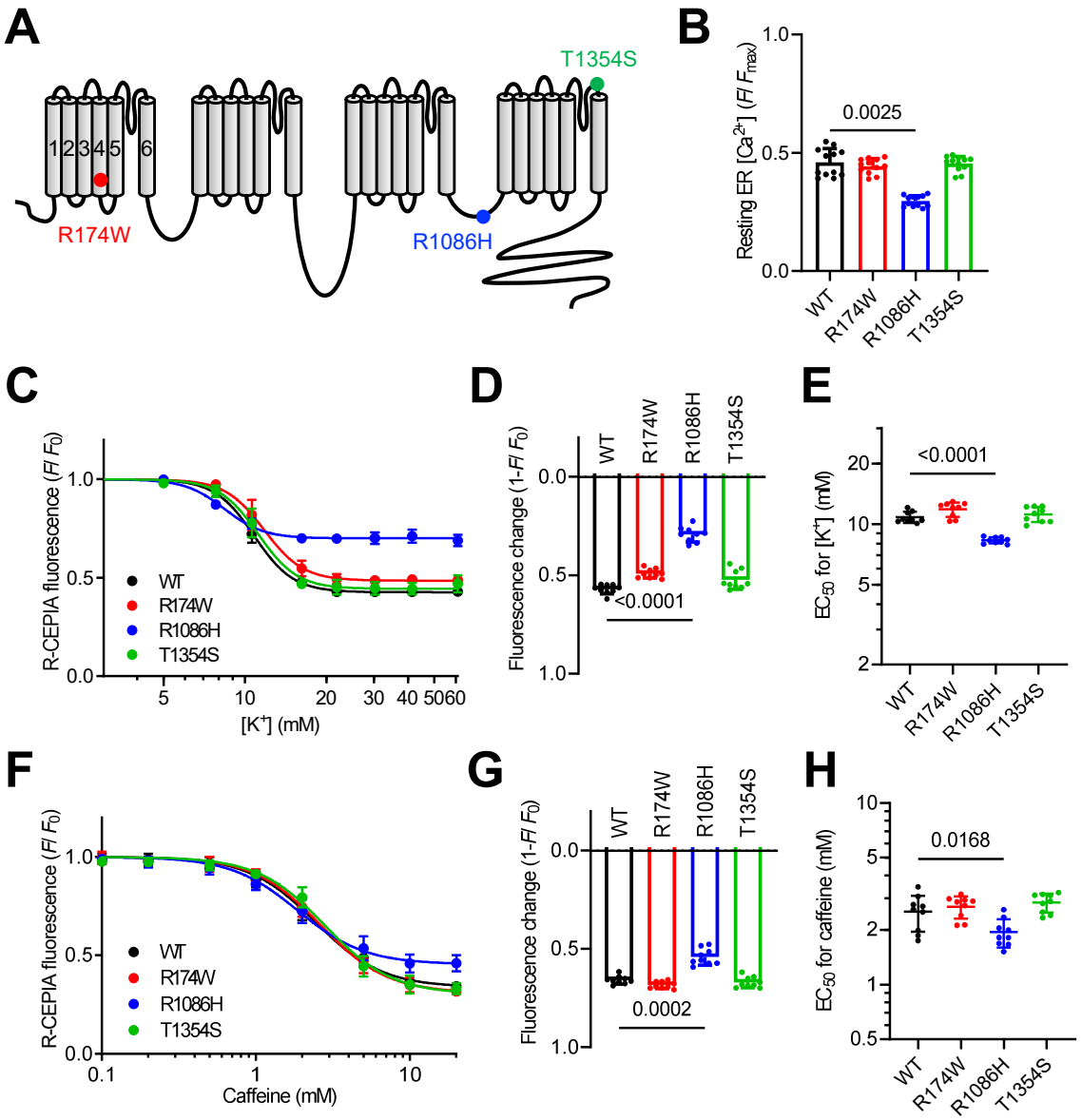

Figure 4 **Effect of MH mutations in Cav1.1 on DICR activity. (A)** Schematic drawing of the location of MH mutations (R174W, R1086H and T1354S) in Cav1.1. **(B)** Resting ER $[Ca^{2+}]$ in cells expressing WT and mutant Cav1.1. Data are means ± SD (n = 12) and were analyzed by one-way ANOVA with Dunnett's multiple comparisons test. **(C)** $[K^+]$ dependence of R-CEPIA1er fluorescence (F/F_0) in WT (black), R174W (red), R1086H (blue) and T1354S (green) Cav1.1 cells. Data are means ± SD (n = 9). **(D, E)** Fluorescence change by 61 mM K^+ (**D**) and EC_{50} values for K^+ (**E**). Data are means ± SD (n = 9) and were analyzed by one-way ANOVA with Dunnett's multiple comparisons test. **(F)** Caffeine dependence of v(F/F_0) in WT (black), R174W (red), R1086H (blue) and T1354S (green) Cav1.1 cells. Data are means ± SD (n = 9). **(G, H)** Fluorescence change by 20 mM caffeine (**G**) and EC_{50} values for caffeine (**H**). Data are means ± SD (n = 9) and were analyzed by one-way ANOVA with Dunnett's multiple comparisons test.

Figure 5

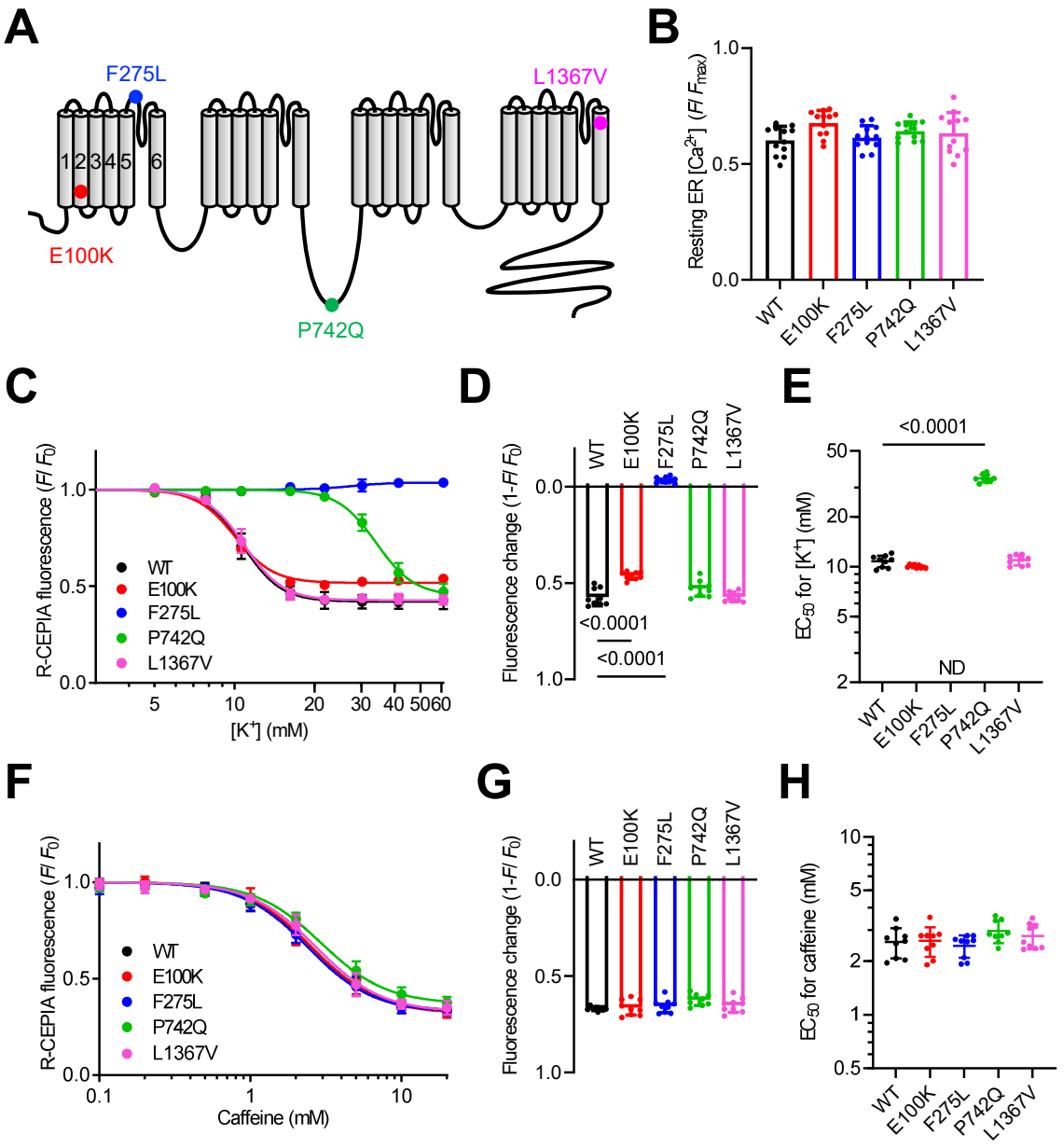

Figure 5 **Effect of myopathy mutations in Cav1.1 on DICR activity. (A)** Schematic drawing of the location of myopathy mutations (E100K, F275L, P742Q and L1367V) in Cav1.1. **(B)** Resting ER [Ca^{2+}] in cells expressing WT and mutant Cav1.1. Data are means ± SD (n = 12) and were analyzed by one-way ANOVA with Dunnett's multiple comparisons test. **(C)** [K^+] dependence of R-CEPIA1er fluorescence (F/F_0) in WT (black), E100K (red), F275L (blue), P742Q (green) and L1367V (magenta) Cav1.1 cells. Data are means ± SD (n = 9). **(D, E)** Fluorescence change by 61 mM K^+ (**D**) and EC_{50} values for K^+ (**E**). Data are means ± SD (n = 9) and were analyzed by one-way ANOVA with Dunnett's multiple comparisons test. **(F)** Caffeine dependence of R-CEPIA1er fluorescence (F/F_0) in WT (black), E100K (red), F275L (blue), P742Q (green) and L1367V (magenta) Cav1.1 cells. Data are means ± SD (n = 9). **(G, H)** Fluorescence change by 20 mM caffeine (**G**) and EC_{50} values for caffeine (**H**). Data are means ± SD (n = 9) and were analyzed by one-way ANOVA with Dunnett's multiple comparisons test.

Figure 6

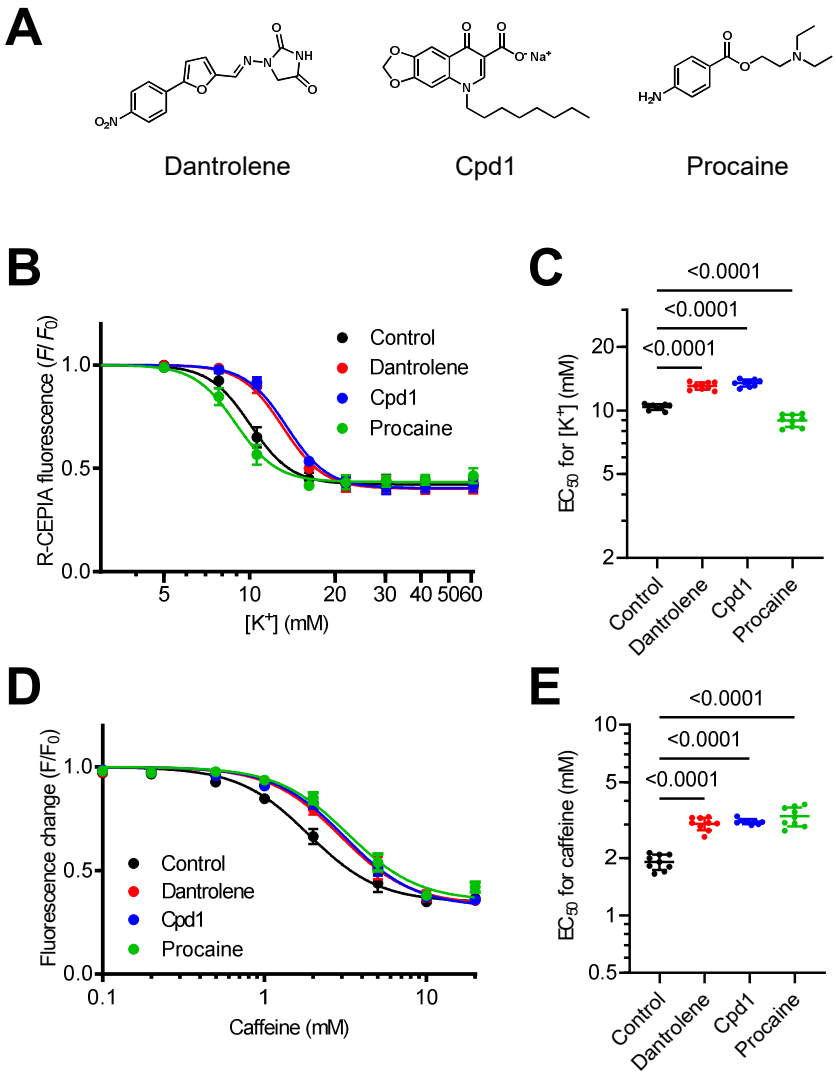

Figure 6 **Effect of RyR1 inhibitors on DICR activity. (A)** Chemical structures of dantrolene, Cpd1 and procaine. **(B)** $[K^+]$ dependence of fluorescence change (F/F_0) in cells without (Control, black) or with dantrolene (10 μM, red), Cpd1 (3 μM, blue) or procaine (5 mM, green). Data are means ± SD (n = 9). **(C)** EC_{50} values for $[K^+]$. Data are means ± SD (n = 9) and were analyzed by one-way ANOVA with Dunnett's multiple comparisons test. **(D)** Caffeine dependence of R-CEPIA1er fluorescence (F/F_0) in cells without (Control, black) or with dantrolene (10 μM, red), Cpd1 (3 μM, blue) or procaine (5 mM, green). Data are means ± SD (n = 9). **(E)** EC_{50} values for caffeine. Data are means ± SD (n = 9) and were analyzed by one-way ANOVA with Dunnett's multiple comparisons test.

Figure 7

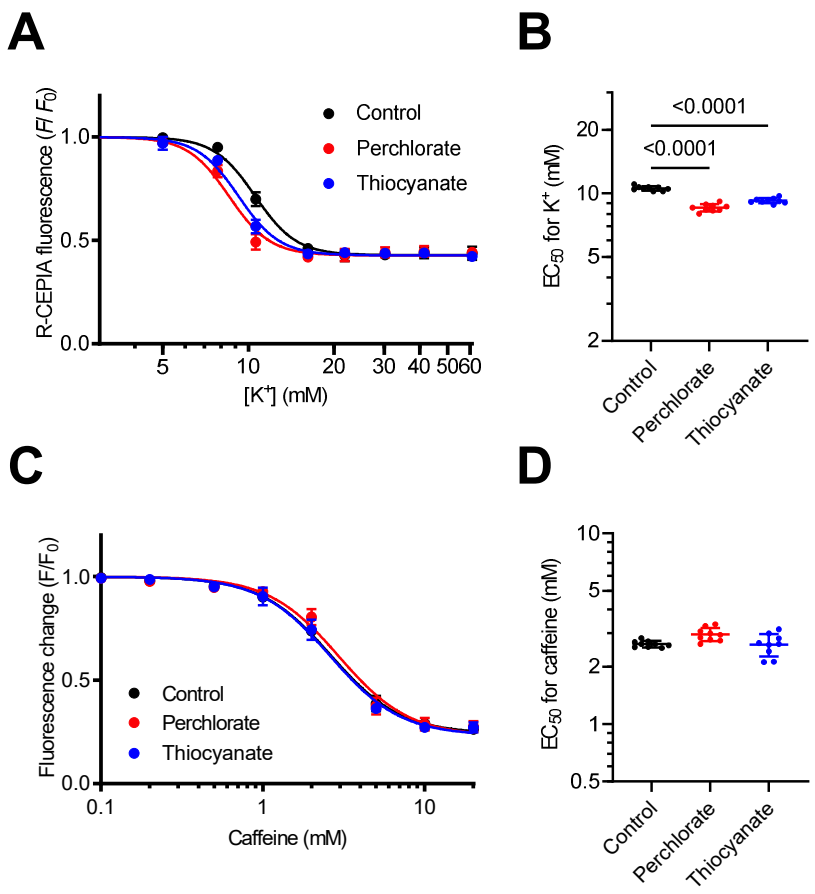

Figure 7 **Effect of lyotropic anions on DICR activity. (A)** [K^+] dependence of fluorescence change (F/F_0) in cells in the absence (Control, black) or presence of perchlorate (10 mM, red) or thiocyanate (10 mM, blue). Data are means ± SD (n = 9). **(B)** EC_{50} values for K^+. Data are means ± SD (n = 9) and were analyzed by one-way ANOVA with Dunnett's multiple comparisons test. **(C)** Caffeine dependence of R-CEPIA1er fluorescence (F/F_0) in cells in the absence (Control, black) or presence of perchlorate (10 mM, red) or thiocyanate (10 mM, blue). Data are means ± SD (n = 9). **(D)** EC_{50} values for caffeine. Data are means ± SD (n = 9) and were analyzed by one-way ANOVA with Dunnett's multiple comparisons test.